EUROPEAN ORGANIZATION FOR NUCLEAR RESEARCH

CERN-EP/87-05

January 7th 1987

MEASUREMENT OF THE STANDARD MODEL PARAMETERS FROM A STUDY OF W AND Z BOSONS

The UA2 Collaboration

Bern[1] - *CERN*[2] - *Copenhagen (NBI)*[3] - *Heidelberg*[4] - *Orsay (LAL)*[5] - *Pavia*[6] - *Perugia*[7] - *Pisa*[8] - *Saclay (CEN)*[9]

R. Ansari[5], P. Bagnaia[2], M. Banner[9], R. Battiston[7], K. Bernlöhr[4], C.N. Booth[2], K. Borer[1], M. Borghini[2], G. Carboni[8], V. Cavasinni[8], P. Cenci[2,a], J.-C. Chollet[5], A.G. Clark[2], C. Conta[6], F. Costantini[8], P. Darriulat[2], B. De Lotto[5], T. Del Prete[8], L. Di Lella[2], J. Dines-Hansen[3], K. Einsweiler[2], L. Fayard[5], R. Ferrari[6], M. Fraternali[6], D. Froidevaux[5], J.-M. Gaillard[5], O. Gildemeister[2], V.G. Goggi[6], C. Gössling[2], B. Hahn[1], H. Hänni[2], J.R. Hansen[2], P. Hansen[3], K. Hara[1], N. Harnew[2], E. Hugentobler[1], E. Iacopini[8,b], L. Iconomidou-Fayard[5], K. Jakobs[4], P. Jenni[2], E.E. Kluge[4], O. Kofoed-Hansen[3], E. Lançon[9], P. Lariccia[8c], B. Lisowski[2,d], M. Livan[6], S. Loucatos[9], B. Madsen[3], B. Mansoulié[9], G.C. Mantovani[7], L. Mapelli[2,e], K. Meier[2], B. Merkel[5], R. Möllerud[3], M. Moniez[5], R. Moning[1], M. Morganti[8], C. Onions[2], T. Pal[2], M.A. Parker[2], G. Parrour[5], F. Pastore[6], M. Pepe[7], Ch. Petridou[2], H. Plothow-Besch[4], M. Polverel[9], L. Rasmussen[2], J.-P. Repellin[5], A. Roussarie[9], V. Ruhlmann[9], G. Sauvage[5], J. Schacher[1], F. Stocker[1f], M. Swartz[2], J. Teiger[9], S.N. Tovey[2,g], W.Y.Tsang[h], M. Valdata-Nappi[8], V. Vercesi[6], A.R. Weidberg[2], M. Wunsch[4], H. Zaccone[9], and J.A. Zakrzewski[2,i].

ABSTRACT

A study has been made of the decays $W \to e\nu$ and $Z \to e^+e^-$, using the UA2 detector at the CERN $\bar{p}p$ Collider. The data correspond to an integrated luminosity of 142 nb^{-1} at a centre-of-mass collision energy $\sqrt{s}$ = 546 GeV, and 768 nb^{-1} at $\sqrt{s}$ = 630 GeV. Measurements of the Standard Model parameters from samples of 251 W decay and 39 Z decay candidates are compared with expectations of the Standard Electroweak Model.

(Submitted to Physics Letters B)

---

1. Laboratorium für Hochenergiephysik, Universität Bern, Sidlerstrasse 5, CH-3012 Bern, Switzerland.

2. CERN, 1211 Geneva 23, Switzerland.

3. Niels Bohr Institute, Blegdamsvej 17, Copenhagen, Denmark.

4. Institut für Hochenergiephysik der Universität Heidelberg, Schröderstrasse 90, 6900 Heidelberg, FRG.

5. Laboratoire de l'Accélérateur Linéaire, Université de Paris-Sud, Orsay, France.

6. Dipartimento di Fisica Nucleare e Teorica, Università di Pavia and INFN, Sezione di Pavia, Via Bassi 6, Pavia, Italy.

7. Gruppo INFN del Dipartimento di Fisica dell'Università di Perugia and INFN, Perugia, Italy.

8. Dipartimento di Fisica dell'Università di Pisa and INFN, Sezione di Pisa, Via Livornese, I-56010 S. Piero a Grado, Pisa, Italy.

9. Centre d'Etudes Nucléaires de Saclay, France.

a) On leave from Scuola Normale Superiore, Pisa and INFN, Perugia, Italy.

b) Also at Scuola Normale Superiore, Pisa, Italy.

1. INTRODUCTION

In previous publications [1-4] we have reported data on the production and decay of the W and Z bosons, via the processes

$$\bar{p} + p \rightarrow W^{\pm} + \text{anything}$$
$$\rightarrow e^{\pm} + \nu_e\,(\bar{\nu}_e) + \text{anything}, \qquad (1)$$

and

$$\bar{p} + p \rightarrow Z + \text{anything}$$
$$\rightarrow e^{+} + e^{-} + \text{anything}. \qquad (2)$$

The data published correspond to a total integrated luminosity of 142 nb^{-1} at a centre-of-mass energy $\sqrt{s}$ = 546 GeV and 316 nb^{-1} at $\sqrt{s}$ = 630 GeV. In a subsequent run during 1985, the integrated luminosity at $\sqrt{s}$ = 630 GeV collected by the UA2 detector was increased to 768 nb^{-1}. In this letter we report final results on those aspects of W and Z production and decay which are relevant to comparisons with the Standard Electroweak Model [5].

In a following publication [6], we report on the production properties of the W and Z bosons, emphasising those aspects related to the predictions of QCD.

2. DATA ANALYSIS AND EVENT SAMPLES

The UA2 detector has been described elsewhere [3-4,7-9]. Of importance for the accurate measurement of the Standard Model parameters using the electron decay modes of the W and Z bosons are :

i. the accurate measurement of the energies of identified electrons, and

ii. the selection with a well-measured efficiency of event samples that are minimally contaminated by backgrounds, generally resulting from hadronic jets that satisfy the criteria used to identify electrons in the detector.

2.1 Calorimeter energy measurements

Electrons are identified in the UA2 detector over the full azimuthal range, $0° < \phi < 360°$, and in polar angles $20° < \theta < 160°$ with respect to the beam line.

The UA2 calorimeter, which is used to measure the electron energy, is divided into two regions. In the central region ($40° < \theta < 140°$) each of 240 electromagnetic and hadronic calorimeter cells subtends 10° in θ and 15° in ϕ [7]. Clusters of energy deposition are obtained by joining cells which share a common side and contain at least 0.4 GeV. The cluster energy E_{cl} is defined as $E_{cl} = E_{em} + E_{had}$, where E_{em} is the sum of the energies deposited in cells of the electromagnetic compartment of the calorimeter and E_{had} is the corresponding sum for the hadronic compartments.

---

c) Also at Dipartimento di Fisica dell'Università di Perugia, Italy.

d) Visitor from Institute of Physics, Polish Academy of Science, Warsaw.

e) On leave from INFN, Pavia, Italy.

f) Present adress : New York State University, Stony Brook, NY, USA.

g) Visitor from the University of Melbourne, Victoria, Australia.

h) Cavendish Laboratory, University of Cambridge, Cambridge, U.K.

i) Visitor from Institute of Physics, University of Warsaw, Poland.

Since the response of the calorimeter to electrons and hadrons is different, two values of the energy are retained, corresponding to whether the calorimeter cluster is considered to result from an electromagnetic or from a hadronic shower.

In the forward calorimeters [8] ($20° < \theta < 37.5°$ and $142.5° < \theta < 160°$), clusters are reconstructed as for the central calorimeter. Since the 240 forward calorimeter cells are far from the interaction point, and their size is large compared with that of an electromagnetic shower, any cluster of electromagnetic origin should consist of at most two adjacent cells. For showers of hadronic origin, the absence of hadronic calorimetry prevents an energy measurement from the calorimeters alone, and information from the momenta of reconstructed charged tracks in the preceding magnetic spectrometer is included.

Each calorimeter cell was initially calibrated in a 10 GeV/c electron beam [8-9], and the energy resolution for isolated electrons was measured to be, on average,

$$\sigma_E \simeq 0.14\sqrt{E} \quad (E \text{ in GeV}).$$

However, the most important energy measurement error results from systematic uncertainties of the calorimeter calibration. The uncertainty on the absolute scale of energy measurement in the central calorimeter, after an operating period exceeding 5 years, is $\pm 1.5\%$, with an additional cell-to-cell calibration uncertainty of rms 2.5%. A further uncertainty results from the time variation of the light attenuation properties of the calorimeter scintillator. We estimate a total systematic uncertainty on the measured electron energy of $\pm 1.6\%$. These estimates have been confirmed by a recalibration of 40 cells of the central calorimeter in June 1986.

In the case of the forward calorimeters, 50 cells were recalibrated in July 1986. As a result of this recalibration, the energy value assigned to forward electrons of the W and Z samples has been changed on average by -4.4%. In particular, we note that the energy has been re-evaluated for the sample of forward electrons collected during the 1985 run, and also for previously published data samples [1-4]. We estimate an uncertainty on the absolute energy scale of $\pm$ 2.5%, with an additional cell-to-cell calibration uncertainty of 2.5%.

2.2 Identification of events satisfying the $W \to e\nu$ hypothesis

Events are selected from a hardware trigger which requires a transverse energy deposition $E_T > 10$ GeV in any 2×2 cell matrix of the electromagnetic calorimeter, in coincidence with a minimum bias signal from small angle hodoscopes [10] which are used to suppress backgrounds not resulting from $p\bar{p}$ collisions.

An electron candidate is defined to be a reconstructed calorimeter cluster of transverse energy $E_T^e > 10$ GeV which satisfies a set of criteria characteristic of isolated high-p_T electrons:

i. the cluster of energy deposition in the calorimeter must have small lateral dimensions and a small energy leakage in the hadronic compartment as expected for an isolated electron,

ii. a charged particle track which points to the cluster must be reconstructed and the pattern of energy deposition in the calorimeter must be consistent with that expected from an isolated electron incident along the track direction,

iii. in the forward directions, the reconstructed track momentum must be consistent with the associated calorimeter energy deposition,

iv. a hit must be recorded in preshower counters located behind $\simeq$ 1.5 radiation length thick converters that precede the calorimeters, and this hit must be aligned with the reconstructed track and have a pulse height characteristic of an electron shower.

Details of the analysis criteria used for electron identification are noted in Refs. [3] and [4]. The efficiency, η, of identifying high-p_T electrons in the region of the central calorimeter is measured from the data themselves to be $\eta = 0.71 \pm 0.07$. In the forward regions, the efficiency is estimated to be $\eta = 0.79 \pm 0.03$.

For each event the neutrino transverse momentum, $\vec{p}_T^{\,\nu}$, is defined to be equal to the missing transverse momentum, $\vec{p}_T^{\,miss}$, which is obtained from the expression

$$\vec{p}_T^{\,miss} = - \vec{p}_T^{\,e} - \Sigma \vec{p}_T^{\,cl} - \vec{p}_T^{\,sp} \qquad (3)$$

where the sum extends over all observed clusters (excluding the electron itself) of transverse energy $E_T^{cl} > 3$ GeV. The vector $\vec{p}_T^{\,sp}$ is the total transverse momentum carried by the system of all other particles not associated with clusters exceeding 3 GeV transverse energy. From measurements of $\vec{p}_T^{\,e}$ and $\vec{p}_T^{\,\nu}$, the transverse mass $m_T^{e\nu}$ is evaluated to be

$$m_T^{e\nu} = \sqrt{[2\, p_T^e\, p_T^\nu\, (1 - \cos\Delta\phi)]} \qquad (4)$$

where $\Delta\phi$ is the angle between $\vec{p}_T^{\,e}$ and $\vec{p}_T^{\,\nu}$.

A total of 5340 events contain at least one electron candidate satisfying $p_T^e > 11$ GeV/c. Figure 1 shows the p_T distribution of the electron candidates in the (p_T^e, p_T^ν) plane, and separately for the p_T^e and p_T^ν projections. If more than one electron candidate is selected, that of largest p_T is retained. In Fig. 1 the $W \to e\nu$ signal is clearly visible as a clustering of events with $p_T^e \simeq p_T^\nu$. Also included in the sample are $Z \to e^+e^-$ events, with large p_T^e and small p_T^ν. The region of low p_T^e is dominated by hadronic background and for this reason we restrict the W sample to electron candidates of $p_T^e > 20$ GeV/c. The resulting $m_T^{e\nu}$ distribution is shown in Fig. 2a. Background contributions from misidentified hadrons or hadronic jets, from $W \to \tau\nu$ decays, and from $Z \to e^+e^-$ decays for which one electron escapes the detector acceptance, are superimposed on this figure. Of all the $W \to e\nu$ decays within the acceptance of the apparatus, 80% are expected to satisfy the kinematic requirements $p_T^e > 20$ GeV/c and $m_T^{e\nu} > 50$ GeV. Therefore these selections have been applied to the final $W \to e\nu$ sample of 251 events used in the studies of Section 3. The p_T^e distribution of this sample is shown in Fig. 2b, again with superimposed background estimates.

In the distributions of Fig. 1 and Fig. 2b, we note the existence of one event containing an electron candidate of $p_T^e = 77.4$ GeV/c. The event has no associated jet activity, and a neutrino with $p_T^\nu \simeq 80$ GeV/c is reconstructed as in Eqn. (3), opposite in azimuth to the electron. The transverse mass is evaluated using Eqn. (4) to be $m_T^{e\nu} \simeq 156$ GeV. Background contributions to this event from two-jet events in which one jet fakes the electron and the second jet is outside the detector acceptance, or from a beam halo particle hitting the calorimeter in coincidence with a genuine $\bar{p}p$ collision, are negligible. However, events of large $m_T^{e\nu}$ are expected via the processes $u\bar{d} \to e^+\nu_e$ or $\bar{u}d \to e^-\bar{\nu}_e$, mediated by W exchange in the s-channel, and we estimate that 0.07 such events should be observed with $p_T^e > 70$ GeV/c in the W sample. This estimate is insensitive, to within $\simeq \pm 10\%$, to the structure function parameterisation used. This event has been excluded from the W event sample for the measurements described in Section 3.

2.3 Identification of $Z \to e^+e^-$ decays

The Z trigger requires the simultaneous presence of two depositions of electromagnetic transverse energy, each exceeding $\simeq$5 GeV, in 2 × 2 - cell matrices separated in azimuth by at least 60°. As for the W trigger, a minimum bias signal is required in coincidence. In the following analysis, clusters are formed as for the W search, and a selection $E_T > 10$ GeV on the cluster transverse energy is made. If the selection criteria used for the W- analysis are used on both clusters of the $Z \to e^+e^-$ candidate, the detection efficiency is low ($\simeq$ 50%). However, because of the increased rejection resulting from the requirement of two clusters of energy with lateral and longitudinal profiles consistent with those of isolated electrons, less stringent selection criteria can be applied while maintaining good Z identification efficiency and good rejection of hadronic background. Using the W sample, we estimate that the efficiency in the central region for the identification of isolated electrons, from the selections noted below, is 14% higher than the efficiency of electron identification quoted in Section 2.2.

In the central region, initial selection is made on the lateral and longitudinal shower profile of each cluster, as in item (i) of Section 2.2. To improve the electron efficiency, the limit on energy leakage into the hadronic compartments of the calorimeter is increased by a factor 1.5. Additional rejection against hadronic background is obtainable from the requirement that the energy deposition due to each electron candidate is well isolated from other calorimetric energy in the event. We require less than 7 GeV within a cone of 30° about the electron candidate. In the forward regions, the electron identification criteria are as described in section 2.2 [3,4]. The resulting distribution of mass, m_{ee}, is shown in Fig. 3a, and the Z peak is clearly visible; the sample includes 54 events satisfying $m_{ee} \geq 76$ GeV, with an estimated background of 14 events. The final sample is obtained by requiring that at least one electron candidate satisfies the criteria (ii) and (iii) of Section 2.2, except that (again to improve the electron efficiency) the requirement of spatial matching between the track and preshower signal is relaxed from d = 10 mm to d = 14 mm and the charge Q of the preshower signal is required to satisfy Q > 2 mip (minimum ionising equivalents). A total of 39 events satisfy $m_{ee} \geq 76$ GeV and are attributed to the Z, with an estimated background of 1.3 events.The distribution of m_{ee} for the final sample is shown in Fig. 3b.

The process of internal bremsstrahlung can produce events of the type $Z \to e^+e^-\gamma$; one such event is included in the final event sample [2-4,12]. This event consists of a 24 GeV photon separated in space by 31° from an electron of 11 GeV. The probability of seeing at least one (eeγ) event having an (eeγ) configuration less likely than that observed in the sample of 39 Z decays is estimated to be $\simeq$ 0.4.

Fig. 1a includes an event containing an isolated electron candidate of $p_T^e = 90.1$ GeV/c. The electron is balanced by a hadronic jet of $E_T = 77 \pm 8$ GeV. A careful examination of the jet topology suggests the overlap of an electron having $p_T^e \simeq 22$ GeV/c with a hadronic jet having $E_T \simeq 52$ GeV. The electron pair mass is then estimated to be $m_{ee} \simeq 91$ GeV. The natural interpretation of this event is therefore the production of a Z having transverse momentum $p_T^Z \simeq 70$ GeV/c, with an associated jet that overlaps one of the electrons from $Z \to e^+e^-$ decay. This event does not pass the calorimetric selections of the Z analysis, and is excluded from the Z sample.

3. PHYSICS RESULTS RELATED TO THE STANDARD MODEL

Using the data samples described in the previous section, we now discuss properties of the data relevant to tests of the Standard Model.

3.1 The W and Z masses and widths. Limits on the number of neutrino types.

An estimate of the W mass, m_W, is obtained from a comparison of the $m_T^{e\nu}$ distribution of Fig. 2a in the range $m_T^{e\nu} > 50$ GeV, with that expected from W decay. Results of the best-fit comparison are superimposed in Fig. 2. A Monte Carlo program is used, which generates the $dN/dm_T^{e\nu}$ distribution for different values of m_W. The distribution of $m_T^{e\nu}$ depends only weakly on the W production mechanism. Nevertheless, the Monte Carlo program takes into account our understanding of W production and decay, and a full simulation of the detector response to $W \to e\nu$ events.

The W longitudinal momentum distribution is obtained from the quark (antiquark) structure functions of the proton (antiproton) as parameterised in Ref. [13]. The W transverse momentum, p_T^W, is generated from the distribution of Ref. [14], which agrees well with the data [6]. The decay is described by standard (V-A) coupling with decay parameters given by the Standard Model.

The best fit to the experimental distribution is

$$m_W = 80.2 \pm 0.6(\text{stat}) \pm 0.5(\text{sys}_1) \pm 1.3(\text{sys}_2)\ \text{GeV}, \qquad (5)$$

and if the W width, Γ_W, is fitted as an additional free parameter, $\Gamma_W < 7$ GeV (90% confidence level). The statistical uncertainty in (5) takes into account the resolution of the energy measurement, and also cell-to-cell uncertainties of the energy calibration. Systematic uncertainties of the mass measurement have two major contributions, which are quoted separately. The uncertainty (sys_1) of Eqn. (5) is mainly due to possible systematic biases in the evaluation of p_T^ν, and consequently $m_T^{e\nu}$. The second systematic uncertainty (sys_2) reflects the measurement uncertainty on the global energy scale of the calorimeter calibration. The influence on the mass fit of the (dominantly low-p_T) background contribution in Fig. 2a is small.

The W mass can alternatively be estimated from a fit to the observed p_T^e distribution of Fig. 2b. In this case, the evaluation is less sensitive to the p_T^ν evaluation, but is more sensitive to the detailed shape of the p_T^W distribution. Selecting a sub-sample of events for which $p_T^W < 15$ GeV/c, the m_W measurement is consistent with the result of (5).

Using a relativistic Breit-Wigner shape modified by the mass resolution, the Z mass is evaluated from a fit to the mass values of a sub-sample of 25 events for which both electron energies are accurately measured and for which $m_{ee} > 76$ GeV. The result is

$$m_Z = 91.5 \pm 1.2(\text{stat}) \pm 1.7(\text{syst})\ \text{GeV}, \qquad (6)$$

where the systematic uncertainty results mainly from the calorimeter energy scale uncertainty of the central and forward calorimeters. From (5) and (6), we measure

$$m_Z - m_W = 11.3 \pm 1.3(\text{stat}) \pm 0.5(\text{sys}_1) \pm 0.8(\text{sys}_2)\ \text{GeV}, \qquad (7)$$

where (sys_1) again results from systematic uncertainties of the P_T^ν evaluation in (5), and (sys_2) reflects the differing global energy scale uncertainties of the forward and central calorimeters.

A direct measurement of the width, Γ_Z, of the Z is difficult since a precise knowledge of the shape of the mass resolution is required. The average measurement error is estimated to be 3.1 GeV, which is of the same order as the expected Z width. Following [4], we obtain

$$\Gamma_Z = 2.7 \pm 2.0(\text{stat}) \pm 1.0(\text{syst})\ \text{GeV}$$

$$< 5.6\ \text{GeV (90\% confidence level)},$$

where the quoted systematic error reflects the uncertainty of the average measurement error. These measurements are in good agreement with previously published results [4], and with measurements from the UA1 Collaboration [15].

As described in Ref. [4], we can obtain an independent but model-dependent [16] estimate of the ratio of total widths, Γ_Z/Γ_W, from

$$\Gamma_Z/\Gamma_W = R^{exp} \quad R^{th} \quad R^{lept},$$

where $R^{exp} = \sigma_W{}^{e\nu}/\sigma_Z{}^{ee}$ is the experimentally determined cross-section ratio from this experiment, where R^{th} is the ratio σ_Z/σ_W obtained theoretically, and $R^{lept} = \Gamma_Z{}^{ee}/\Gamma_W{}^{e\nu}$ is the ratio of leptonic partial widths as evaluated from the Standard Model. We measure [6]

$$\begin{aligned} R^{exp} &= 7.2^{+1.7}_{-1.2} \text{ (stat)}, \\ &< 9.52 \text{ (90\% confidence level)}, \\ &< 10.42 \text{ (95\% confidence level)}. \end{aligned} \tag{8}$$

Both R^{th} and R^{lept} depend on $\sin^2\theta_W$, explicitly through the neutral current couplings and implicitly via the W and Z masses. However the product $R^{th}R^{lept}$ is constant to within 1% over the range $\sin^2\theta_W = 0.232 \pm 0.009$ (see Eqn. 14). A more important uncertainty results from the use of different sets of structure functions in the theoretical calculation of R^{th} [14,17]. Recent estimates [18] give values of R^{th} ranging between 0.285 and 0.325. Using R^{exp} as in (8), and the value $R^{th} = 0.305 \pm 0.020$, we evaluate

$$\begin{aligned} \Gamma_Z/\Gamma_W &= 0.82^{+0.19}_{-0.14} \text{ (stat)} \pm 0.06 \text{ (theor)}, \\ &< 1.09 \pm 0.07 \text{ (theor)} \quad \text{(90\% confidence level)}, \\ &< 1.19 \pm 0.08 \text{ (theor)} \quad \text{(95\% confidence level)}, \end{aligned} \tag{9}$$

where the theoretical error reflects the uncertainty on R^{th} as quoted above.

The ratio of total widths is sensitive to both the number of neutrino types and the mass of the top quark, m_t [19]. Assuming that the charged members of any new family and also any other unknown particle are too massive to contribute significantly to W or to Z decays, we obtain the results summarized in Fig. 4, which shows the expected variation of Γ_Z/Γ_W with m_t if the number of light neutrino types is respectively 3,4 or 7. The error bars at the end of each of these lines shows the effect of varying $\sin^2\theta_W$ in the range 0.232 ± 0.009. Also shown in Fig. 4 are the experimental evaluations of Γ_Z/Γ_W as given in (9). From the 95% confidence limit using the conservative upper estimate of $R^{th} = 0.325$, the data exclude more than seven neutrino types when no requirement is made on m_t. This limit decreases to three neutrino types in the case $m_t > 74$ GeV.

3.2 Measurement of the Standard Model parameters

The masses of the weak bosons, m_W and m_Z, are two essential parameters of the Standard Model. In its minimal expression, it relates them to the fine structure constant α, the Fermi constant G_F and the weak mixing angle θ_W via the following relations [21]:

$$m_W{}^2 = A^2/[(1 - \Delta r)\sin^2\theta_W] \tag{10}$$

$$m_Z{}^2 = A^2/[(1 - \Delta r)\sin^2\theta_W\cos^2\theta_W] \tag{11}$$

where [22] :

$$A = (\pi\alpha/\sqrt{2}G_F)^{1/2} = 37.2810 \pm 0.0003 \text{ GeV}.$$

In relations (10) and (11), the quantity Δr accounts for the effects of one-loop radiative corrections on the W and Z masses and has been computed to be [21,23-24]

$$\Delta r = 0.0711 \pm 0.0013 \qquad (12)$$

assuming that $m_t = 35$ GeV and that the mass of the Higgs boson is $m_H = 100$ GeV. This quantity is insensitive to m_H but would deviate from (12) if the top quark were very massive ($\Delta r = 0$ for $m_t \simeq 270$ GeV with $\sin^2\theta_W = 0.232$) [24-26].

From a measurement of the ratio m_W/m_Z, which is free from the common systematic uncertainty of calorimeter energy calibration on the W and Z mass scale, a direct measurement of $\sin^2\theta_W$ is provided via the relation

$$\sin^2\theta_W = 1-(m_W/m_Z)^2. \qquad (13)$$

From Eqn. (13), we evaluate

$$\sin^2\theta_W = 0.232 \pm 0.025(\text{stat}) \pm 0.010(\text{syst})$$

where the quoted uncertainty includes the contribution of a $\pm$ 0.5 GeV systematic error on the value of m_W which is not related to the energy calibration of the calorimeter (see Eqn. 5). This result is independent of other experiments, and of theoretical uncertainties.

By using accurate existing measurements of A [22], and the value of Δr in (12), a more precise measurement of $\sin^2\theta_W$ is obtainable from a best fit to Eqns. (10) and (11). We obtain

$$\sin^2\theta_W = 0.232 \pm 0.003(\text{stat}) \pm 0.008(\text{syst}). \qquad (14)$$

These results are in excellent agreement with previously published UA2 and UA1 results [4,15] and with those obtained in low energy neutrino experiments [27-30], which average to :

$$\sin^2\theta_W = 0.232 \pm 0.004(\text{exp}) \pm 0.003(\text{theor}), \qquad (15)$$

where the weighted mean is evaluated on the basis of quoted experimental errors, assuming a charmed quark mass $m_c = 1.5$ GeV, and ignoring the uncertainty on the theoretical error due to m_c.

The results are summarized in Fig. 5 where correlations between uncertainties of the m_W and m_Z measurements are shown in the $[m_Z, (m_Z - m_W)]$ plane.

Any departure from the minimal Standard Model will induce modifications to the above formalism. In particular values of $\sin^2\theta_W$ deduced from Eqn. (10), from Eqn. (13), or from low energy neutrino experiments, will generally differ. All existing measurements are in excellent agreement with the predictions of the minimal Standard Model; nevertheless, they can be used to place limits on possible deviations from the minimal Standard Model. In particular the quantity [31]

$$\rho = \frac{m_W^2}{m_Z^2\cos^2\theta_W} \qquad (16)$$

is sensitive to the Higgs sector (more precisely it depends on the isospin structure of the Higgs fields, but only weakly on their masses). Assuming the value of Δr in (12), we measure from (16)

$$\rho = 1.001 \pm 0.028(\text{stat}) \pm 0.006(\text{syst}),$$

in good agreement with the minimal Standard Model prediction of $\rho = 1$.

The relations (10) and (11) may also be used to measure the radiative correction parameter Δr, which may deviate [24-26] from its calculated value in (12) if, for example, a new fermion family existed with a large mass splitting within isospin doublets, or if there existed additional gauge bosons, or if as noted above the top quark were very massive. Eliminating $\sin^2\theta_W$ from Eqns. (10) and (11) we obtain

$$1 - \Delta r = (A^2/m_W{}^2)/(1 - [m_W{}^2/m_Z{}^2]),$$

from which we deduce

$$\Delta r = 0.068 \pm 0.087(\text{stat}) \pm 0.030(\text{syst}), \qquad (17)$$

in agreement with the minimal Standard Model prediction of (12). The value of $\sin^2\theta_W$ in (15), from low energy experiments, can be used in equations (10) and (11) to provide a more accurate measurement of Δr. We measure

$$\Delta r = 0.068 \pm 0.022(\text{stat}) \pm 0.032(\text{syst}). \qquad (18)$$

We therefore conclude that the existing data are consistent with, but barely sensitive to, the existence of radiative corrections from known processes (see Fig. 5).

3.3 Charge asymmetry of the decay $W \to e\nu$

The magnetic spectrometers of the UA2 detector allow a measurement of the electric charge in the forward regions ($20° < \theta < 37.5°$ and $142.5° < \theta < 160°$) where a distinctive charge asymmetry is expected in $W \to e\nu$ decay [4]. Assuming a universal (V-xA) coupling of the W to fermions, the electron (positron) angular distribution takes the form

$$dn/d(\cos\theta^*) \propto (1 - q\cos\theta^*)^2 + 2q\alpha\cos\theta^* \qquad (19)$$

where the angle θ^* is measured with respect to the incident proton in the W rest frame, where q is the sign of the electron or positron charge, and

$$\alpha = [(1 - x^2)/(1 + x^2)]^2. \qquad (20)$$

The sensitivity of the asymmetry measurement to the exact form of the angular distribution is largest for values of $\cos\theta^*$ close to ± 1, corresponding to small values of $p_T{}^e$. Therefore, we relax the $m_T{}^{e\nu}$ cut of Section 2.2 and consider all electron candidates with $p_T{}^e > 20$ GeV/c and $m_T{}^{e\nu} > 40$ GeV that are detected in the forward regions. This leaves a total of 47 events with an estimated background of 4.2 ± 0.3 events from misidentified hadrons. The $W \to \tau\nu$ and Z decay contaminations of this sample are estimated to be respectively 0.6 events and 1.2 events.

A unique value of $\cos\theta^*$ is not calculable for W decays because the longitudinal neutrino momentum, $p_L{}^\nu$, is not measured. The requirement $m_{e\nu} = m_W$ results in two solutions for $p_L{}^\nu$. For events in which both solutions are allowed, the solution corresponding to the smaller absolute value of

the W longitudinal momentum is chosen. Seven events, which because of the limited measurement accuracy satisfy $m_T^{e\nu} > m_W$, are excluded from the analysis. Furthermore, transformations of the electron four-momentum to the W rest frame are unique only if $p_T^W = 0$, and the quarks have no transverse momentum. For $p_T^W \neq 0$ the initial parton directions are not known and the convention of Ref. [32] is used.

A Monte Carlo program is used to correct the $\cos\theta^*$ distribution for the effects of the detector acceptance and resolution. The background-subtracted and acceptance-corrected $\cos\theta^*$ distribution is shown in Fig. 6 and is consistent with the expected form $(1 - q\cos\theta^*)^2$ of Eqn. (19) with $\alpha = 0$, modified to take into account higher-order QCD contributions to W production [11].

To extract a value of α from these data we use a Monte Carlo program to compare the expected two dimensional distributions $f^{\pm}(p_T^e, \theta_e)$, for positrons and electrons separately, with those observed. Following the analysis of [4], we measure α to be consistent with zero, as expected for V-A coupling. We determine $\alpha < 0.35$ (90% confidence level), corresponding in Eqn. (20) to $0.51 < |x| < 1.97$.

4. CONCLUSIONS

We have described measurements of the Standard Model parameters, using the final UA2 data samples for the processes

$$\bar{p} + p \rightarrow W^{\pm} + \text{anything}$$
$$\rightarrow e^{\pm} + \nu_e\,(\bar{\nu}_e) + \text{anything, and}$$

$$\bar{p} + p \rightarrow Z + \text{anything}$$
$$\rightarrow e^+ + e^- + \text{anything.}$$

The measured boson masses are

$$m_W = 80.2 \pm 0.6(\text{stat}) \pm 0.5(\text{sys}_1) \pm 1.3(\text{sys}_2)\ \text{GeV},$$

where (sys_1) is a systematic uncertainty which results mainly from possible systematic biases in the evaluation of p_T^{ν}, and (sys_2) is from the energy scale uncertainty, and

$$m_Z = 91.5 \pm 1.2(\text{stat}) \pm 1.7(\text{syst})\ \text{GeV},$$

with the systematic uncertainty resulting in this case from the energy scale uncertainty. The values are, within errors, consistent with previously published values [4] and with published data of the UA1 experiment [15]. From the above measurements of m_W and m_Z we evaluate

$$\sin^2\theta_W = 0.232 \pm 0.025(\text{stat}) \pm 0.010(\text{syst}).$$

If in addition accurate low-energy measurements of α and G_F are used, together with recent calculations of the radiative correction Δr, we obtain

$$\sin^2\theta_W = 0.232 \pm 0.003(\text{stat}) \pm 0.008(\text{syst}).$$

There is no evidence of deviations from the predictions of the minimal Standard Model. If deviations are expressed in terms of the parameter ρ ($= 1$ in the minimal Standard Model), we obtain

$$\rho = 1.001 \pm 0.028(\text{stat}) \pm 0.006(\text{syst}).$$

Furthermore, the existing data are consistent with (but barely sensitive to) the expected contributions to the Standard Model parameters from known radiative corrections, even if recent low-energy neutrino measurements are taken into account.

From measurements of the ratio of the boson widths, Γ_Z/Γ_W, we describe model-dependent limits on the number of neutrino types allowed by the existing data. Within 95% confidence limits, the data allow up to seven neutrino types if no restriction is placed on the top mass m_t. A limit of three neutrino types is obtained for the case $m_t > 74$ GeV.

ACKNOWLEDGEMENTS

This experiment would have been impossible without the very successful operation of the CERN $\bar{p}p$ Collider whose staffs and coordinators we acknowledge for their collective effort.

We thank the technical staffs of the institutes collaborating in UA2 for their important contributions to maintain and improve the performance of the detector.

We are grateful to the UA4 Collaboration for providing the signals from their small-angle scintillator arrays and to the UA5 Collaboration for the loan of scintillator hodoscopes.

Financial support from the Schweizerischer Nationalfonds zur Förderung der Wissenschaftlichen Forschung to the Bern group, from the Danish Natural Science Research Council to the Niels Bohr Institute group, from the Bundesministerium für Forschung und Technologie to the Heidelberg group, from the Institut National de Physique Nucléaire et de Physique des Particules to the Orsay group, from the Istituto Nazionale di Fisica Nucleare to the Pavia, Perugia and Pisa groups and from the Institut de Recherche Fondamentale (CEA) to the Saclay group are acknowledged.

REFERENCES

1. UA2 Collaboration. M. Banner et al., Phys. Lett. **122B** (1983) 476.

2. UA2 Collaboration. P. Bagnaia et al., Phys. Lett. **129B** (1983) 130.

3. UA2 Collaboration. P. Bagnaia et al., Z. Phys. C - Particles and Fields **24** (1984) 1.

4. UA2 Collaboration. J. Appel et al., Z. Phys. C - Particles and fields **30** (1986) 1.

5. S.L. Glashow, Nucl. Phys. **22** (1961) 579 ;
   S. Weinberg, Phys. Rev. Lett. **19** (1967) 1264 ;
   A. Salam, Proc. of the 8th Nobel Symposium, Aspenäsgarden, 1968, p.367 (Almqvist and Wiksell, Stockholm).

6. UA2 Collaboration. R. Ansari et al., to be published.

7. For 18% of data collected at $\sqrt{s} = 546$ GeV, a 60° azimuthal region of the central calorimeter was replaced by a magnetic spectrometer followed by a lead glass wall. See Refs. [1] to [3].

8. UA2 Collaboration. B. Mansoulié : The UA2 apparatus at the CERN $\bar{p}p$ Collider, Proc. of the 3rd Moriond Workshop on $\bar{p}p$ Physics (1983) p. 609, éditions Frontières 1983 ;
   M. Dialinas et al., LAL Orsay preprint LAL-RT/83-14 ;
   K. Borer et al., Nucl. Inst. Meth. **227** (1984) 29.

9. A. Beer et al., Nucl. Inst. Meth. **224** (1984) 360.

10. UA4 Collaboration. M. Bozzo et al., Phys. Lett. **147B** (1984) 392.

11. S.D. Ellis, R. Kleiss and W.J. Stirling, Phys. Lett. **154B** (1985) 435.
    R. Kleiss and W.J. Stirling, Nucl. Phys. **B262** (1985) 235.

12. Similar events have been reported by the UA1 Collaboration. See G. Arnison et al., Phys. Lett. **135B** (1984) 250.

13. M. Glück et al., Z. Phys. C - Particles and Fields **13** (1982) 119.

14. G. Altarelli, R.K. Ellis, M. Greco and G. Martinelli, Nucl. Phys. **B246** (1984) 12 ;
    G. Altarelli, R.K. Ellis and G. Martinelli, Z. Phys. C - Particles and Fields **27** (1985) 617.

15. UA1 Collaboration. G. Arnison et al., Phys. Lett. **166B** (1985) 484.

16. F. Halzen and K. Mursula, Phys. Rev. Lett. **51** (1983) 857 ;
    K. Hikasa, Phys. Rev. **D29** (1984) 1939.

17. N. G. Deshpande et al., Phys. Rev. Lett. **54** (1985) 1757.

18. M. Diemoz and G. Martinelli, private communication.

19. J. H. Kühn et al., Nucl. Phys. **B272** (1986) 560 ;
    D. Yu Bardin et al., Z. Phys. C - Particles and Fields **32** (1986) 121.

20. See L. Dobrzynski, Proc. Intl. Conf. on Physics in Collision, Autun, 1985, p25.
    Editions Frontieres, ed. B. Aubert and L. Montanet.
    See also references therein.

21. A. Sirlin, Phys. Rev **D22** (1980) 971 ;
W.J. Marciano, Phys. Rev. **D20** (1979) 274 ;
M. Veltman, Phys. Lett. **91B** (1980) 95 ;
F. Antonelli et al., Phys. Lett. **91B** (1980) 90.

22. Particle Data Group, Phys. Lett. **170B** (1986) 1.

23. F. Jegerlehner, Bielefeld preprint BI-TP 1986/8 ;
W. Hollick, DESY preprint DESY 86-049 (1986).

24. W.J. Marciano and A. Sirlin, Phys. Rev. **D29** (1984) 945 ;
W.J. Marciano and A. Sirlin, Phys. Rev. **D22** (1980) 2695.

25. M. Veltman, Nucl. Phys. **B123** (1977) 89.

26. Z. Hioki, Nucl. Phys. **B229** (1983) 284 ;
R.G. Stuart, CERN preprint CERN-TH/4342 (1985).

27. CDHSW Collaboration. H. Abramowicz et al., Phys. Rev. Lett. **57** (1986) 298.

28. CHARM Collaboration. J.V. Allaby et al., Phys. Lett. **177B** (1986) 446.

29. CCFR Collaboration, presented by F. Merrit. Proc. of the 12th.
Intl. Conf. on Neutrino Physics and Astrophysics, Sendai, Japan, June 1986.
To be published.

30. FMMF Collaboration, presented by R. Brock. Proc. of the 12th.
Intl. Conf. on Neutrino Physics and Astrophysics, Sendai, Japan, June 1986.
To be published.

31. D. Ross and J. Veltman, Nucl. Phys. **B95** (1975) 135 ;
P.Q. Hung and J.J. Sakurai, Nucl. Phys. **B143** (1978) 81.

32. J.C. Collins and D.E. Soper, Nucl. Phys. **B197** (1982) 446.

FIGURE CAPTIONS

1. The distribution (a) in the (p_T^e,p_T^ν) plane of 5340 events containing at least one electron candidate of $p_T^e > 11$ GeV/c. If more than one electron candidate is identified, that of highest p_T is selected. The superimposed line represents $p_T^\nu = p_T^e$. In (b), the p_T^e projection is plotted and in (c) the p_T^ν projection is shown for all events, and for 722 events satisfying $p_T^e > 20$ GeV/c (shaded).

2. Transverse mass and transverse momentum spectra for the final event sample. The expectation for W decay is evaluated using $m_W = 80.2$ GeV.

   a. The $m_T^{e\nu}$ spectrum of 722 events satisfying $p_T^e > 20$ GeV/c. The expected signal from $W \to e\nu$ decay is superimposed (--). Also shown (-.-.-.-) is the summed contribution from $W \to \tau\nu$ decays (5.2 ± 0.5 events) and from Z decays with one electron outside the UA2 acceptance (9.6 ± 1.6 events). The solid line shows the total of all expected contributions to the $m_T^{e\nu}$ spectrum, including the hadronic background contribution (11.6 ± 2.1 events for $m_T^{e\nu} > 50$ GeV).

   b. The distribution of p_T^e for 251 events satisfying $m_T^{e\nu} > 50$ GeV. The superimposed background contributions are as for (a).

3. The distribution of m_{ee} in events for which at least two electron candidates are identified. In (a), only calorimetric selections are applied, while in (b) at least one electron candidate is required to satisfy track criteria as explained in the text. The contribution of QCD background processes is superimposed (----). The hatched region shows the m_{ee} distribution of the sample of 25 events used in the evaluation of the Z^0 mass.

4. The value of Γ_Z/Γ_W measured by the UA2 experiment (_____), with superimposed statistical and theoretical uncertainties (full and dashed lines respectively). The 95% confidence limit is also shown (------), with superimposed theoretical uncertainties. The expected variation with m_t is shown as a solid line for 3,4 and 7 types of light neutrino. The superimposed error bars represent uncertainties of the theoretical evaluation (see text). The shaded region marks the lower limit on m_t ($m_t > 23$ GeV) as measured at PETRA [20].

5. Confidence contours (68% level) in the ($m_Z - m_W$,m_Z) plane taking into account the statistical error only (i), and with statistical and systematic errors combined in quadrature (ii). The region (a) is allowed by the average of recent low-energy measurements [27-30]. Curve (b) is the Standard Model prediction for $\rho = 1$ with known radiative corrections, and curve (c) is the expectation without radiative corrections.

6. The distribution $dN/d(q\cos\theta^*)$ of well measured W decays for which the charge ($q = -1$ for electrons) is determined, and where θ^* is the angle between the charged lepton and the incident proton in the W rest frame. The data are corrected for acceptance, resolution and background, and the superimposed expectation for W decay takes account of higher order QCD effects.

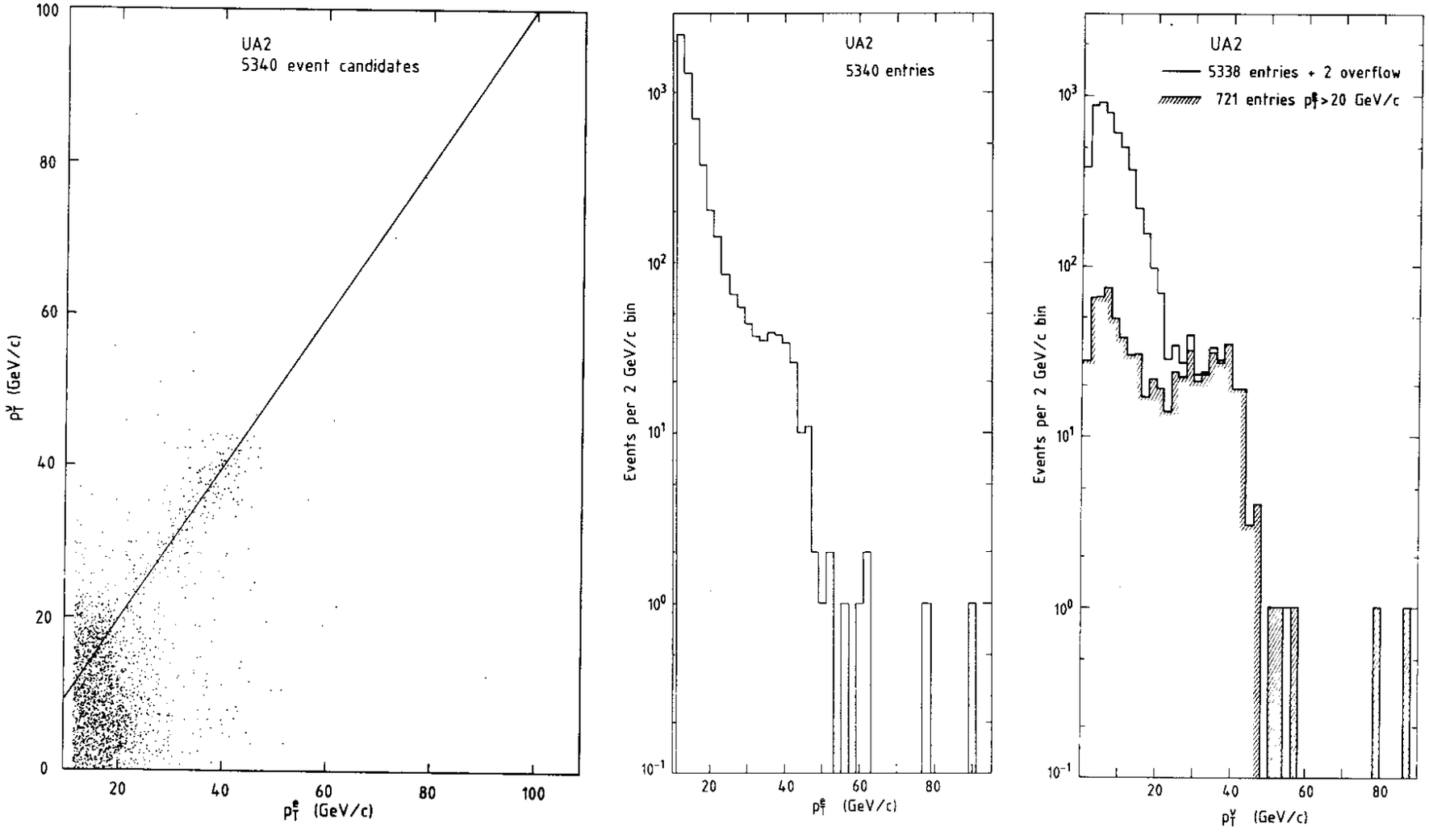
UA2
5340 event candidates
p_T^{ν} (GeV/c)
p_T^{e} (GeV/c)
UA2
5340 entries
Events per 2 GeV/c bin
p_T^{e} (GeV/c)
UA2
5338 entries + 2 overflow
721 entries p_T^{e}>20 GeV/c
Events per 2 GeV/c bin
p_T^{ν} (GeV/c)

Fig. 1

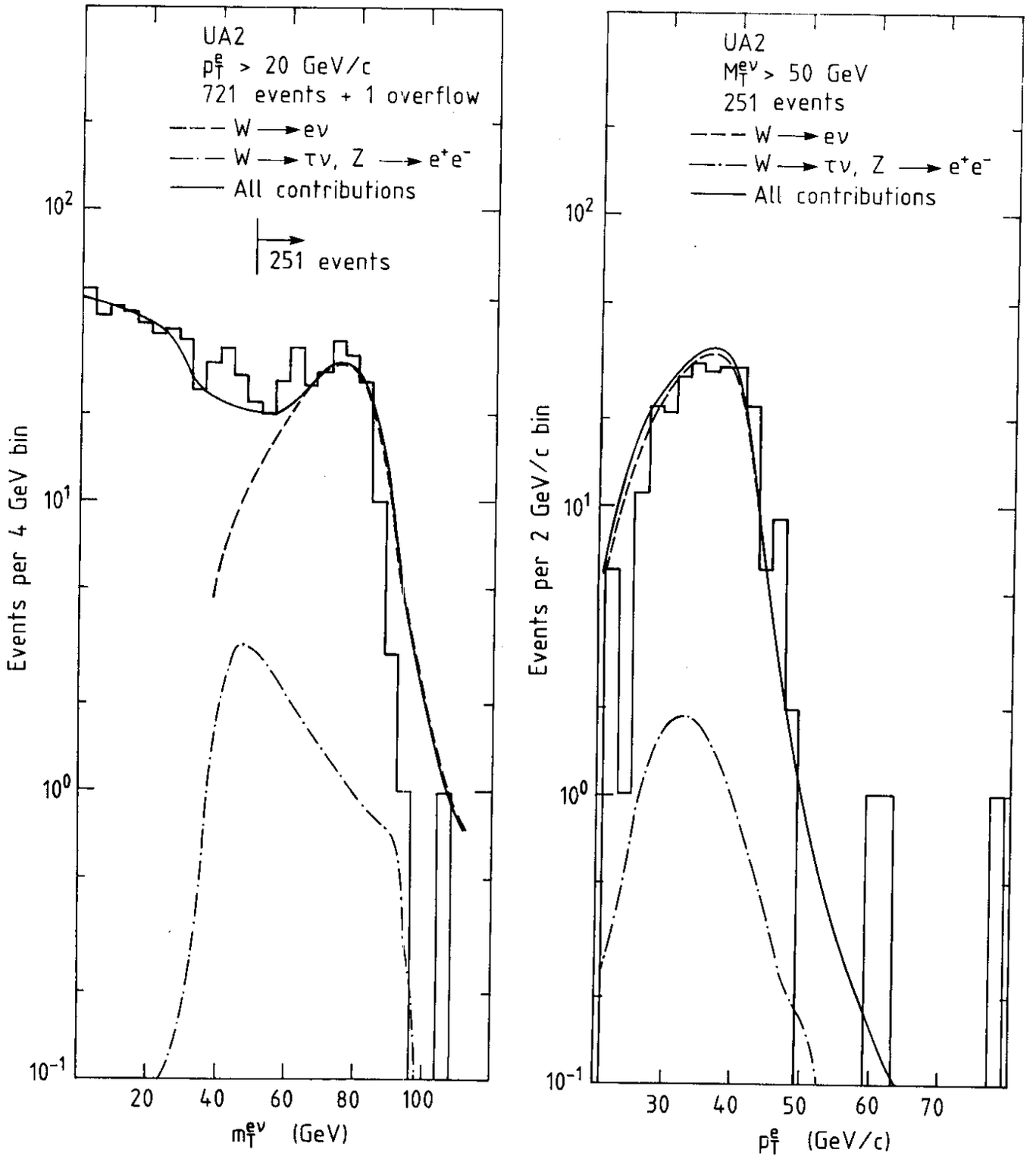
UA2
p_T^e > 20 GeV/c
721 events + 1 overflow
W → eν
W → τν, Z → e⁺e⁻
All contributions
251 events
Events per 4 GeV bin
$m_T^{e\nu}$ (GeV)
UA2
$M_T^{e\nu}$ > 50 GeV
251 events
W → eν
W → τν, Z → e⁺e⁻
All contributions
Events per 2 GeV/c bin
p_T^e (GeV/c)

Fig. 2

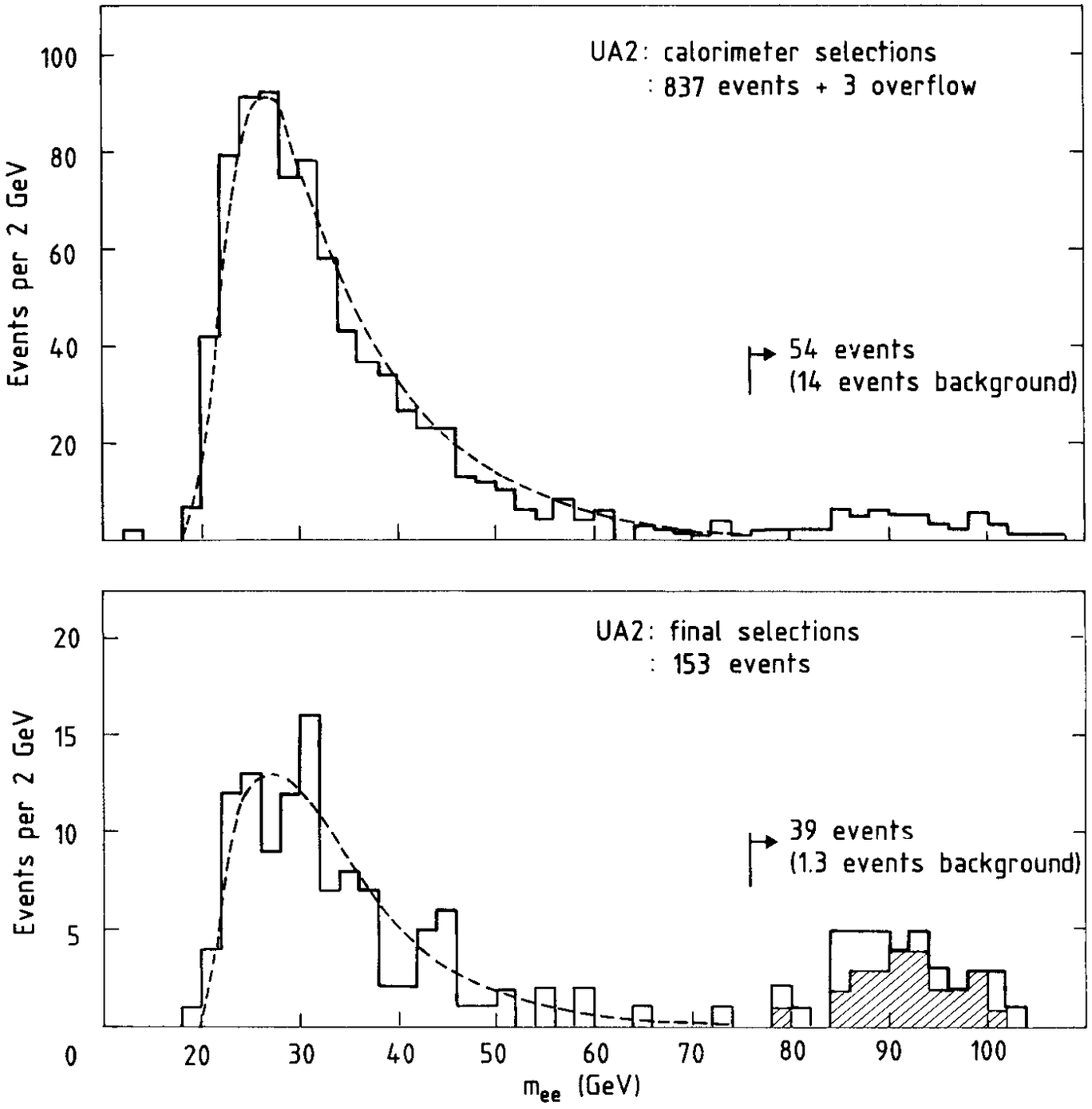
UA2: calorimeter selections
: 837 events + 3 overflow
54 events
(14 events background)
Events per 2 GeV
100
80
60
40
20
UA2: final selections
: 153 events
39 events
(1.3 events background)
Events per 2 GeV
20
15
10
5
0
20
30
40
50
60
70
80
90
100
m_{ee} (GeV)

Fig. 3

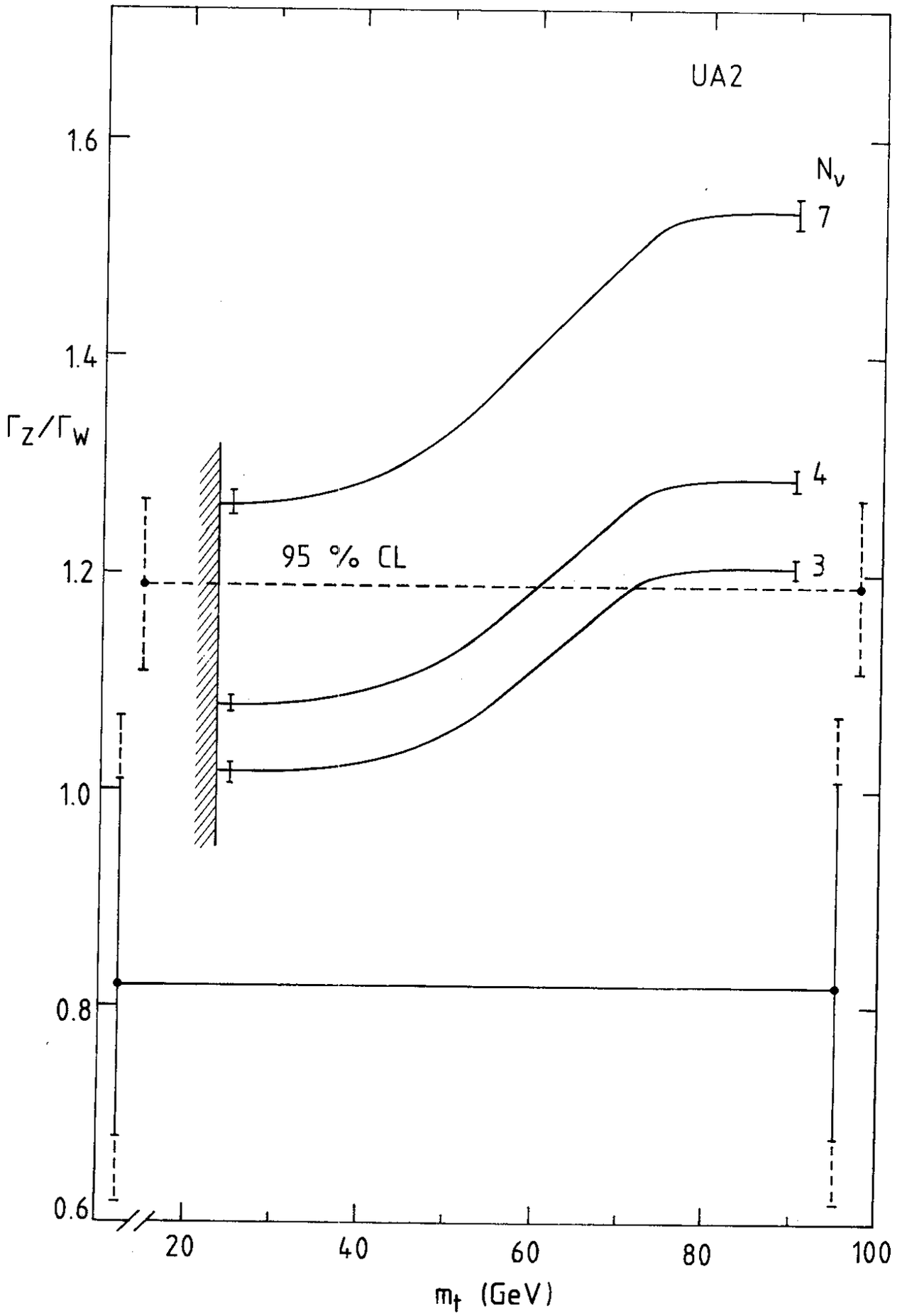
UA2
1.6
1.4
1.2
1.0
0.8
0.6
Γ_Z/Γ_W
N_ν
7
4
3
95 % CL
20
40
60
80
100
m_t (GeV)

Fig. 4

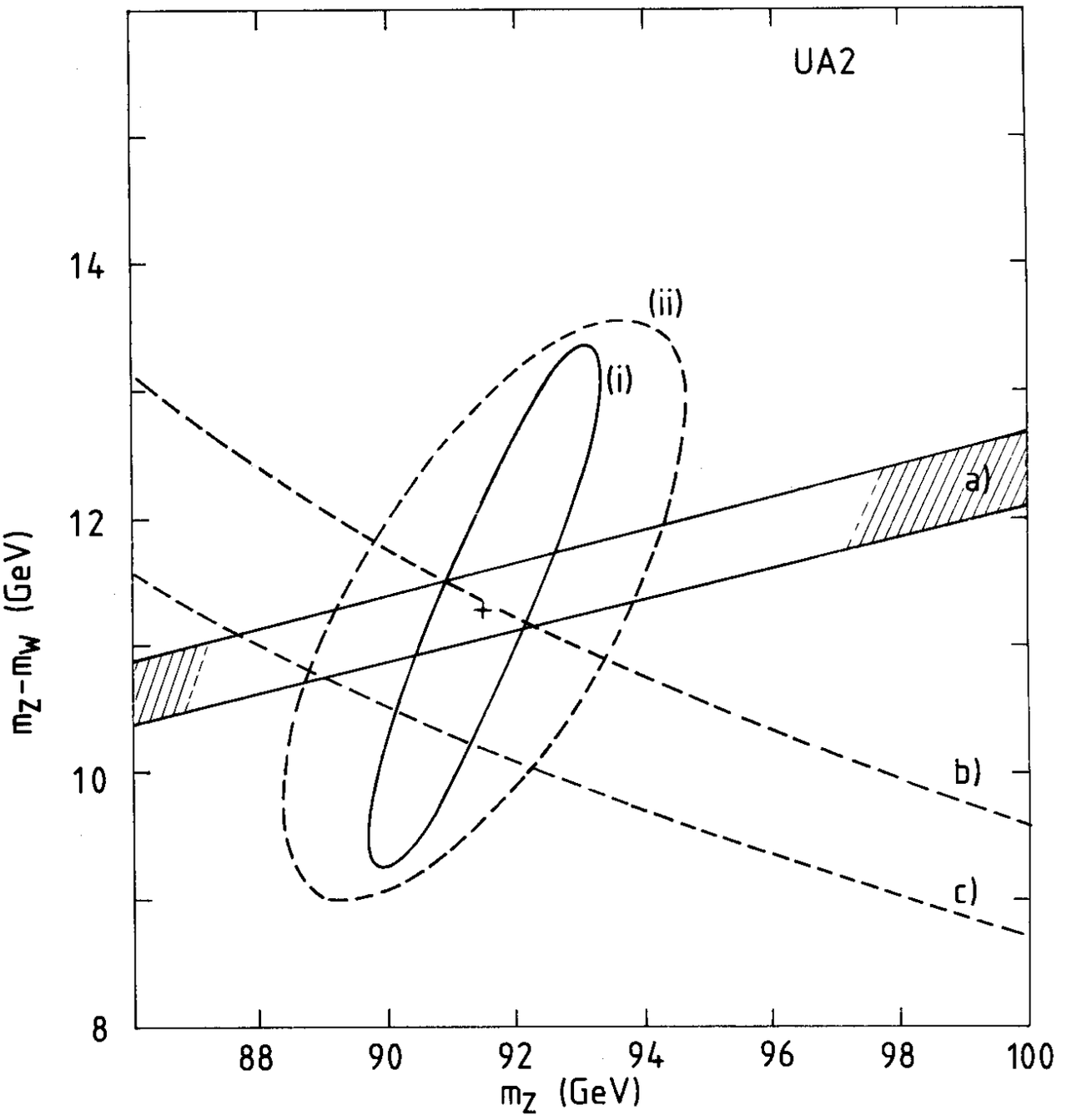

Fig. 5

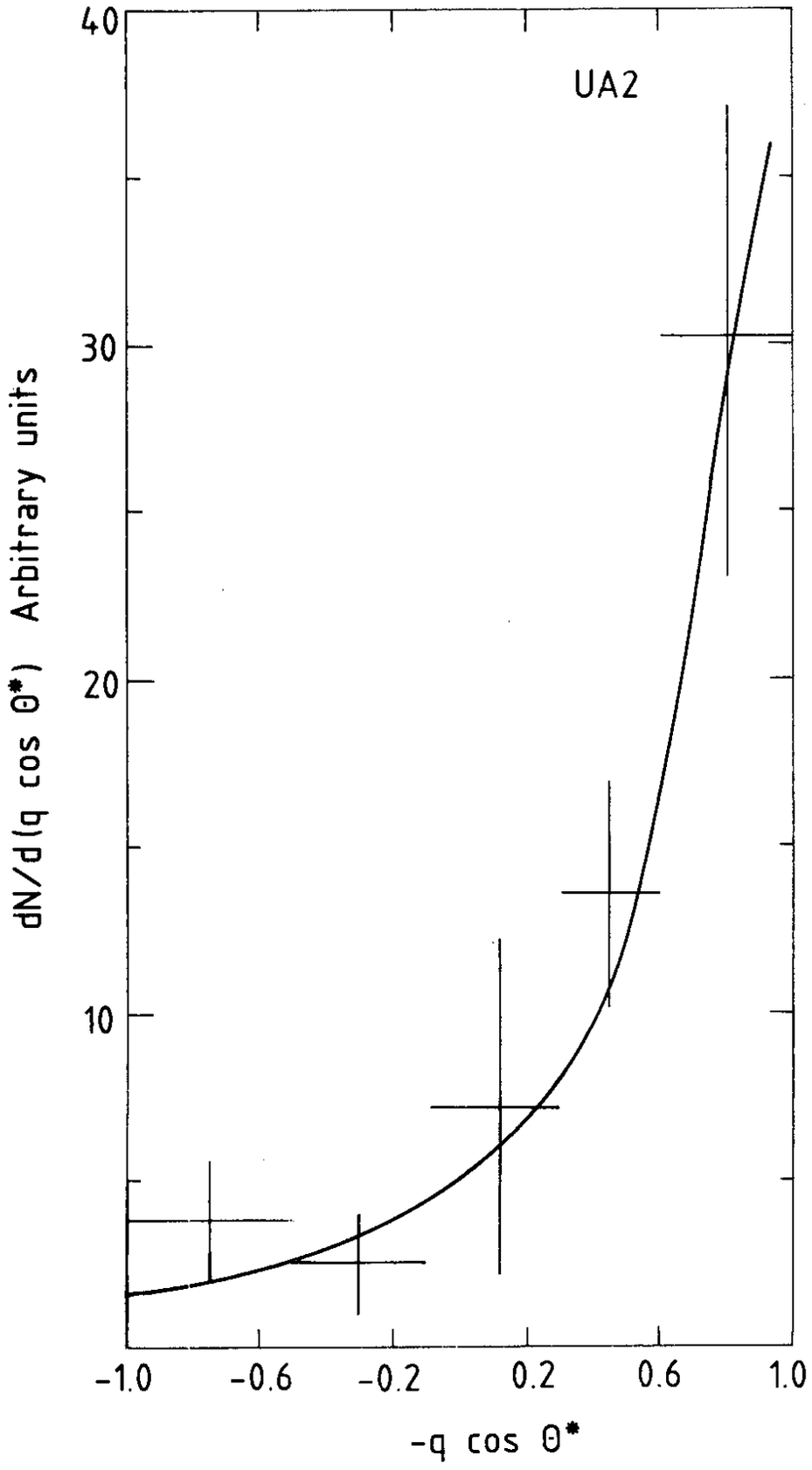
UA2
40
30
20
10
dN/d(q cos θ*) Arbitrary units
-1.0
-0.6
-0.2
0.2
0.6
1.0
-q cos θ*

Fig. 6